Beryllium Oxide Nanotubes and their Connection to the Flat Monolayer

ARTICLE *in* THE JOURNAL OF PHYSICAL CHEMISTRY C · JUNE 2013

Impact Factor: 4.77 · DOI: 10.1021/jp402340z

5 AUTHORS, INCLUDING:

Alessandro Erba
Università degli Studi di Torino
51 PUBLICATIONS **579** CITATIONS
SEE PROFILE

Michel Rérat
Université de Pau et des Pays de l'Adour
134 PUBLICATIONS **1,936** CITATIONS
SEE PROFILE

Roberto Dovesi
Università degli Studi di Torino
337 PUBLICATIONS **11,168** CITATIONS
SEE PROFILE

THE JOURNAL OF PHYSICAL CHEMISTRY C

Article

pubs.acs.org/JPCC

Beryllium Oxide Nanotubes and their Connection to the Flat Monolayer

J. Baima,[†] A. Erba,[†] M. Rérat,[‡] R. Orlando,[†] and R. Dovesi*,[†]

[†]Dipartimento di Chimica and Centre of Excellence NIS (Nanostructured Interfaces and Surfaces), Università di Torino, via Giuria 5, IT-10125 Torino, Italy

[‡]Equipe de Chimie Physique, IPREM UMR5254, Université de Pau et des Pays de l'Adour, FR-64000 Pau, France

ABSTRACT: Single-walled zigzag beryllium oxide (BeO) nanotubes are simulated with an ab initio quantum chemical method. The (n,0) family is investigated in the range from n = 8 (32 atoms in the unit cell and tube radius R = 3.4 Å) to 64 (256 atoms in the cell and R = 27.1 Å). The trend toward the hexagonal monolayer (h-BeO) in the limit of large tube radius R is explored for a variety of properties: rolling energy, elastic modulus, piezoelectric constant, vibration frequencies, infrared (IR) intensities, oscillator strengths, and electronic and nuclear contributions to the polarizability tensor. Three sets of IR-active phonon bands are found in the spectrum. The first one lies in the 0−300 cm^{-1} frequency range and exhibits a very peculiar behavior: the vibration frequencies do tend regularly toward zero when R increases while their IR intensities do not; the nature of these normal modes is unveiled by establishing a connection between them and the elastic and piezoelectric constants of h-BeO. The second (680−730 cm^{-1}) and third (1000−1200 cm^{-1}) sets tend regularly, but with quite different slope, to the optical modes of the h-BeO layer. The vibrational contribution of these modes to the two components (parallel and perpendicular) of the polarizability tensor is also discussed. Simulations are performed using the CRYSTAL program which fully exploits the rich symmetry of this class of one-dimensional periodic systems: 4n symmetry operators for the general (n,0) tube.

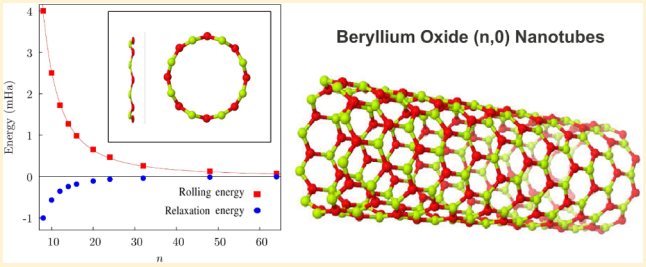

1. INTRODUCTION

Since their discovery,[1] carbon nanotubes (CNTs) have attracted the attention of the scientific community for their unique electrical, mechanical, and thermal properties.[2] The search for noncarbon nanotubes started soon after in the domain of highly anisotropic layered phases such as hexagonal boron nitride (BN) and transition metal disulfides, which can also adopt cage-like structures such as fullerenes.[3−5] Indeed, it is known that inorganic compounds overcome one of the main problems in the technological use of CNTs, that is, the dramatic dependence of their electronic properties on rolling direction and tube diameter. Nowadays, part of the interest in nanotubes is redirected to isotropic semiconducting and inorganic materials.[6] Among these, metal oxides stand out as some of the most versatile compounds, with possible applications ranging from microelectronics to catalysis and chemical sensors production.[7,8]

In this respect, beryllium oxide (BeO) is an interesting material, which constitutes an intermediate case between ionic compounds and semiconducting binary materials such as BN or ZnO.[9,10] In contrast with other alkaline earth oxides, crystalline BeO shows many typical properties of covalent solids: beryllium and oxygen atoms are bound together by sp^3 hybridized bonds in a compact wurzite-type structure. It combines insulating behavior (band gap of ∼10.6 eV) with very high thermal conductivity and high melting point, so it is often used as a refractory material in metallurgy or as a heat-removing insulator in electronics.[11,12] A graphitic metastable layered phase, analogous to the stable hexagonal BN, was also predicted.[13]

Recently, BeO nanotubes have been proposed as rolled up monolayers that are isoelectronic to carbon and BN nanotubes and exhibit the same structure, with the main difference being the increased polarity of the bond.[14] A larger band gap and properties weakly dependent on nanotube radius and chirality—even more so than for BN nanotubes—can be expected. It has been suggested that BeO nanotubes can be synthesized by plasma-chemical reaction or through chemical vapor deposition,[14] a method that has successfully been applied to other metal oxide nanotubes.[7,8]

Recent theoretical investigations, performed within the Density Functional Theory (DFT) with linear density approximation (LDA) and self-interaction corrected LDA, confirm their insulating character and mechanical properties comparable to those of CNTs.[14,15] The effect of impurities and defects has been investigated theoretically,[16,17] as well as their adsorption properties[18] and optical response in the high-frequency range.[19]

In the present work we study the properties of BeO nanotubes of the (n,0) family (from n = 8 to 64) through ab

Received: March 7, 2013
Revised: May 24, 2013
Published: May 29, 2013

initio quantum mechanical simulations performed with the hybrid B3LYP (Becke, three-parameter, Lee−Yang−Parr) functional.[20,21] The same approach has been successfully applied to the investigation of CNTs,[22,23] BN nanotubes,[24−27] ZnO nanotubes,[28] imogolite,[29] and chrysotile.[30] Recent improvements in the CRYSTAL program permit us to fully exploit the symmetry of the system (the point group contains as many symmetry operators as there are atoms in the unit cell, up to 64 × 4 = 256 for the n = 64 tube) and to drastically reduce the computational cost. Thus, we are now able to extend our simulations to larger tube diameters with respect to calculations reported in the literature so far,[15] and, as a consequence, to improve the description of the convergence of a variety of tube properties to those of the corresponding flat monolayer. The total energy and its difference with respect to the BeO hexagonal monolayer (h-BeO), relaxation geometries and energies, elastic moduli and piezoelectric constants, vibrational frequencies, and infrared (IR) intensities are all investigated as a function of n. The polarizability of the tube (electronic and nuclear contribution) is also explored. Some emphasis is given on the relative speed with which each property converges to the corresponding value of the monolayer. All the above-mentioned properties but the elastic one are here computed and discussed for the first time in the literature as concerns BeO nanotubes. From the accurate simulation of these convergences, some connections are discussed between physical properties of nanotubes and the flat monolayer: the relationship between a particular set of IR-active vibration modes of the nanotubes, with vanishing vibration frequency as a function of n, and the elastic and piezoelectric constants of h-BeO is illustrated and discussed.

The paper is organized as follows. A detailed description of the methodological and computational setup used is presented in Section 2, in particular as regards the calculation of the vibration frequencies and related properties with a full exploitation of symmetry. Results are presented and discussed in Section 3, and conclusions are drawn in Section 4.

2. COMPUTATIONAL METHOD

All the calculations reported in the paper are performed with the program CRYSTAL for ab initio quantum chemistry of solid state.[31,32] An all-electron atom-centered Gaussian-type-orbital basis set (BS) is adopted in conjunction with the popular hybrid functional B3LYP.[20,21] The BS used has been obtained by partially splitting the sp contractions and reoptimizing the outermost exponents of a standard 6-311G* split-valence BS: the exponents, in bohr^{-2}, of the most diffuse functions are 0.1222 and 0.5580 for sp and d Be orbitals and 0.2720 and 1.2500 for sp and d O orbitals. The adopted BS is reported on the CRYSTAL Web site.[33]

The level of accuracy in evaluating the infinite Coulomb and Hartree−Fock exchange series is controlled by five parameters,[31] for which values of 8,8,8,8,16 are used. The threshold determining the energy convergence of the self-consistent-field (SCF) step of the procedure is set to 10^{-9} hartree for geometry optimizations, 10^{-10} hartree for the calculation of the electronic contribution to the polarizabilities, and 10^{-11} hartree for the calculation of vibrational frequencies and IR intensities. Reciprocal space is sampled according to a sublattice with shrinking factor set to 8, corresponding to 5, 10, and 50 independent $\vec{k}$-points in the irreducible part of the first Brillouin zone in the nanotubes, monolayer, and bulk BeO, respectively. The DFT exchange-correlation contribution to the energy is evaluated by numerical integration over the unit cell volume. The most accurate predefined pruned grid available in the CRYSTAL program (namely, XXLGRID keyword) is used for numerical integration whose accuracy can be estimated by the error in the electronic charge per unit cell: 2.5×10^{-4} |e| out of a total of 384 |e| for the (16,0) BeO nanotube, for instance.

All the structures have been optimized by using analytical energy gradients with respect to both atomic coordinates and lattice parameters,[34−36] with a quasi-Newton scheme combined with the BFGS algorithm for Hessian updating.[37−40] The convergence of the optimization has been checked on both gradient components and nuclear displacements, for which the default values are chosen.[31]

The calculation of the vibrational frequencies at the Γ point (i.e., at the center of the first Brillouin zone; $\vec{k} = \vec{0}$) is performed within the harmonic approximation; the mass-weighted Hessian matrix **W** is constructed by numerical differentiation of the analytical gradients with respect to the atomic Cartesian coordinates:

$$W^{\Gamma}_{ai,bj} = \frac{1}{\sqrt{M_a M_b}}\left(\frac{\partial^2 E}{\partial r_{ai}\partial r_{bj}}\right) \tag{1}$$

where M_a and M_b are the atomic masses of atoms a and b and r_{ai} is the displacement of atom a from its equilibrium position along the i-th Cartesian direction. Details on the calculation of vibrational frequencies with CRYSTAL can be found elsewhere[41,42] as well as some examples of application.[43−45] Integrated intensities for IR absorption $\mathcal{I}_p$ are computed for each mode p by means of the mass-weighted effective mode Born charge vector $\vec{Z}_p$,[46,47] evaluated through a Berry phase approach:[48,49]

$$\mathcal{I}_p = \frac{\pi}{3}\frac{N_A}{c^2}\cdot d_p \cdot |\vec{Z}_p|^2 \tag{2}$$

with

$$|\vec{Z}_p|^2 = \left|\frac{\partial}{\partial Q_p}\vec{\mu}\right|^2 \tag{3}$$

where N_A is Avogadro's number, c the speed of light, d_p the degeneracy of the p-th mode, $\vec{\mu}$ the cell dipole moment, and Q_p the normal mode displacement coordinate. More details on the calculation of the infrared intensities can be found elsewhere.[50]

The electronic contribution to the static polarizability is evaluated through a Coupled-Perturbed Kohn−Sham/Hartree−Fock (CPKS/HF) scheme[51] adapted to periodic systems.[52] This is a perturbative, self-consistent method that focuses on the description of the relaxation of the crystalline orbitals under the effect of an external electric field. The perturbed wave function is then used to calculate the dielectric properties as energy derivatives. The reader who might be interested in both the method and its implementation in the CRYSTAL code can find all the details elsewhere.[26,53−56] The total static polarizability α^0 is the sum of the electronic and the vibrational contributions:

$$\alpha^0_{ij} = \alpha^{el}_{ij} + \alpha^{vib}_{ij} = \alpha^{el}_{ij} + \sum_p \frac{Z_{p,i}Z_{p,j}}{\nu_p^2} \tag{4}$$

where ν_p is the vibrational frequency of the mode p and $i,j = x, y, z$ label Cartesian directions.

dx.doi.org/10.1021/jp402340z | J. Phys. Chem. C 2013, 117, 12864−12872

The elements of the elastic tensor, for 3D systems, are usually defined as:[57]

$$C_{vu} = \frac{1}{V}\frac{\partial^2 E}{\partial \varepsilon_v \partial \varepsilon_u}\bigg|_0 \quad (5)$$

where ε is the rank-2 symmetric tensor of pure strain and Voigt's notation is used according to which v,u = 1, ..., 6 (1 = xx, 2 = yy, 3 = zz, 4 = yz, 5 = xz, 6 = xy).[58] Since volume V is not defined for 1D and 2D systems, it is here omitted (length or surface could be used instead) and all the elements involving nonperiodic directions (y,z for 1D and z for 2D systems) are null by definition.

The piezoelectric tensor e elements (rank-3) can be defined as (in Voigt's notation):[59,60]

$$e_{iv} = \frac{\partial P_i}{\partial \varepsilon_v}\bigg|_0 \quad (6)$$

where $\vec{P}$ is the polarization (i = 1, 2, 3) and the derivative is calculated at zero strain. In CRYSTAL the polarization can be computed either via localized Wannier functions or via the Berry phase (BP) approach.[49] The latter scheme is used in the present study. Again, since the volume is not defined for 1D and 2D systems, here the polarization $\vec{P}$ reduces to a dipole moment.

3. RESULTS AND DISCUSSION

Bulk and Monolayer. In this section we briefly discuss structural, electronic, and vibrational properties of BeO in its bulk form, that is, with a wurzite-type structure, and flat monolayer form with hexagonal symmetry. The structure of the bulk, slab, and (10,0) nanotube of BeO are graphically compared in Figure 1. The data reported in this section will serve as a reference in the next ones.

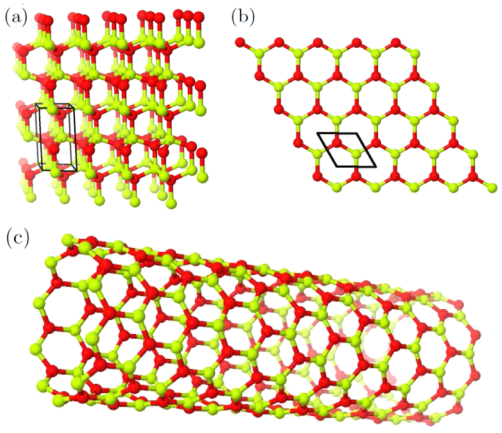

Figure 1. Graphical representation of the structure of (a) the 3D wurzite-like BeO, (b) the h-BeO monolayer, and (c) the (10,0) BeO nanotube. These pictures have been prepared by using the J-ICE online interface to Jmol.[61].

The calculated lattice parameters for the bulk are a = 2.701 Å and c = 4.383 Å, corresponding to a Be−O distance of 1.649 Å. In the monolayer, the bond distance shrinks to 4% to 1.537 Å, corresponding to a lattice parameter a = 2.662 Å. The polarity of the bond in h-BeO is also found to be reduced with respect to the bulk with atomic Born charges changing from 1.84 |e| to 1.52 |e|. The calculated electronic band gap in the bulk is 10.1 eV, to be compared with an experimental value of 10.6 eV,[62] while for the slab an indirect gap of 9.6 eV and a Γ direct gap of 10.2 eV are predicted. The energy difference between bulk and monolayer is 7.16 mHa per BeO formula unit.

The IR spectrum of the bulk consists of two modes: a nondegenerate and a 2-fold degenerate. The longitudinal (transverse) optical frequencies are 682 (1109) and 725 (1123) cm^{-1} and the corresponding IR intensities 1192 and 2256 km/mol, respectively. The Γ vibration modes for the flat monolayer are three: a nondegenerate mode at 721 cm^{-1} and two degenerate modes at 1016 cm^{-1}, with intensities of 48 and 1371 km/mol, respectively.

The electronic polarizability of the bulk is almost isotropic, with $\alpha^e_{xx} = \alpha^e_{yy}$ = 1.974 Å^3 and α^e_{zz} = 2.030 Å^3. A certain degree of anisotropy appears in the static total polarizability tensor: $\alpha^0_{xx} = \alpha^0_{yy}$ = 4.742 while α^0_{zz} = 5.308 Å^3. The in-plane polarizability of h-BeO is somehow similar to the one of the bulk: $\alpha^e_{\parallel}$ = 2.254 Å^3 and $\alpha^0_{\parallel}$ = 4.925 Å^3. Conversely, the out-of-plane polarizability is much lower: $\alpha^e_{\perp}$ = 0.708 Å^3 and $\alpha^0_{\perp}$ = 1.076 Å^3.

Elastic and piezoelectric constants of h-BeO have been computed with the automated algorithms implemented in the CRYSTAL program.[57] The nonzero components of the elastic tensor of the monolayer are $C_{11} = C_{22}$ = 2.223 Ha, C_{12} = 0.810 Ha, and $C_{66} = 1/2(C_{11} - C_{12})$ = 0.707 Ha. The only independent component of the piezoelectric tensor is $e_{11} = -e_{12} = -e_{26}$ = 0.926 |e| × bohr; here units follow from neglecting the volume (not defined in a 2D system) in the definition of elastic and piezoelectric constants.

Structure and Stability. The formation of a BeO nanotube is endothermic. The energy cost of its formation is quantified by the rolling energy ΔE, defined as the difference between the energy of the relaxed tube and that of the relaxed monolayer. The rolling energy can be separated in a positive contribution, the cost of constructing the unrelaxed tube simply by rolling up the relaxed monolayer, and a negative contribution resulting from the subsequent relaxation. We then define the relaxation energy of the tube, δE, as the difference between the energies of the relaxed and unrelaxed tube structures.

Both quantities are reported in Figure 2 as a function of n. For the smallest tube (n = 8) δE is about 1 mHa per BeO unit,

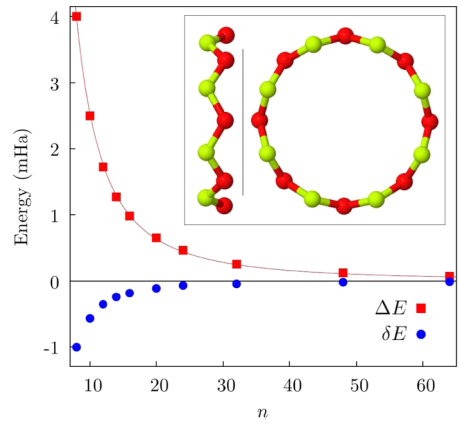

Figure 2. Rolling energy ΔE with respect to the slab (red squares) and geometrical relaxation energy δE (blue circles) of BeO nanotubes of the (n,0) family as a function of n. All energies are reported per BeO unit. For the rolling energy, the result of a fitting with the function $\Delta E = a/n^2$ is shown as well. The inset shows the effect of the structural relaxation as concerns Be and O subrings for the (8,0) nanotube (side and front views).

dx.doi.org/10.1021/jp402340z | J. Phys. Chem. C 2013, 117, 12864−12872

Table 1. Calculated Properties of the $(n,0)$ Series of BeO Nanotubes and BeO Monolayer (h-BeO)[a]

									$\alpha^{\parallel}$		$\alpha^{\perp}$	
n	δE	ΔE	R_u	R_{Be}	R_O	BG	Y_s	e	α^e	α^0	α^e	α^0
8	−1007	4003	3.389	3.412	3.473	9.09	0.130	−1.452	2.265	5.034	1.166	1.874
10	−571	2501	4.236	4.255	4.302	9.32	0.132	−1.380	2.262	5.012	1.194	1.948
12	−358	1722	5.083	5.099	5.138	9.38	0.134	−1.337	2.260	5.001	1.219	2.019
14	−246	1269	5.930	5.944	5.977	9.43	0.135	−1.316	2.259	4.994	1.240	2.084
16	−187	982	6.777	6.790	6.819	9.47	0.135	−1.299	2.258	4.990	1.259	2.143
20	−113	652	8.472	8.482	8.505	9.50	0.136	−1.282	2.257	4.984	1.289	2.245
24	−79	463	10.166	10.175	10.194	9.51	0.136	−1.273	2.256	4.982	1.312	2.328
32	−44	254	13.555	13.561	13.575	9.53	0.136	−1.264	2.255	4.976	1.345	2.452
48	−19	124	20.332	20.337	20.347	9.54	0.137	−1.258	2.255	4.976	1.383	2.611
64	−11	71	27.110	27.114	27.121	9.55	0.137	−1.257	2.254	4.973	1.405	2.703
∞						9.58	0.137	−1.255	2.253	4.971	1.476	3.065
Monolayer						9.62	0.137	−1.263	2.254	4.982	1.481	3.088

[a] δE and ΔE are the relaxation and rolling energies, respectively (see text for a definition); their values are in μHa per BeO unit. R_u is the unrelaxed radius of the tube; R_{Be} and R_O are the radii of the Be and O subrings after relaxation (in Å). The band gap (BG) is reported in eV. Y_s is the modified elastic modulus in TPa × nm and e is the piezoelectric constant in au (|e|× bohr) per BeO unit. $\alpha^{\parallel}$ and $\alpha^{\perp}$ are the longitudinal and transverse components of the electronic α^e and static α^0 polarizabilities per BeO unit (in Å^3). The last row reports the $n \to \infty$ limit deduced from monolayer properties; see the text for the derivation in the case of elasticity and polarizabilities.

then it rapidly decreases: at n = 64 it is 2 orders of magnitude smaller, 11 μHa. The rolling energy ΔE turns out to be four to five times larger than δE and exhibits a clear $1/n^2$ behavior; in order to highlight this aspect, the rolling energy has been fitted to the function $\Delta E = a/n^2$ and the results reported in Figure 2. This behavior is in agreement with the predictions of the classical theory of elasticity,[63] as already noticed for carbon nanotubes.[64] While at n = 8 ΔE has a value that is comparable with the energy difference between bulk and monolayer, at n = 64 it is almost negligible, 71 μHa.

The explicit values of ΔE and δE for each n are reported in Table 1. The rolling energies of the BeO nanotubes are found to be lower, at comparable radii, than those reported for BN nanotubes.[26] This is promising for actual production of BeO nanotubes, although we also notice that the formation of BeO monolayers from bulk crystals is unfavorable with respect to the BN case.

Structure parameters are also reported in Table 1. For each n, the unrelaxed tube radius R_u (as obtained simply by rolling up the monolayer without allowing any atomic relaxation) is reported as well as R_{Be} and R_O that represent the radii of Be and O subrings after atomic relaxation. Relaxation is relatively small in all cases, with the exception of the smallest tubes. Both Be and O atoms tend to move outward, in order to reduce the strain. For n = 8, the radius of the Be subring increases by 0.02 Å whereas O atoms move further by 0.06 Å, in order to reduce steric repulsion due to enhanced population of valence atomic orbitals; the inset in Figure 2 shows the effect of structural relaxation as concerns Be and O subrings for the (8,0) nanotube. For large tubes, Be−O interatomic distances are the same as in the slab (1.537 Å), while for the smallest tubes the two inequivalent distances have a slightly different length (the difference being 0.01 Å for the n = 8 tube, for instance) with the resulting formation of BeO units which are separated from one another. Lattice parameters are stable within 5‰, and correspond to $\sqrt{3}a$, where a is the monolayer lattice parameter. Ionicity of Be−O bonds can be estimated by means of the Born charges which increase from about 1.3 |e| for n = 8 to 1.5 |e| for n = 64, already at the h-BeO limit.

Elasticity and Piezoelectricity. A technologically interesting and widely discussed feature of nanotubes is their response to uniaxial strain along the nanotube axis.[2,65] This property is described by Young's modulus:

$$Y = \frac{1}{V}\frac{\partial^2 E}{\partial \varepsilon^2}\bigg|_{\varepsilon=0} \tag{7}$$

where ε is the applied strain. This expression looks a bit ambiguous in the case of nanotubes where the definition of the volume V requires a conventional choice for the thickness of a monatomic layer. Different conventions for the shell thickness have been among the main causes of the scattered values obtained for Young's moduli in the early studies of carbon nanotubes. An alternative definition that is independent of shell thickness was introduced by Hernández et al.:[65]

$$Y_S = \frac{1}{S}\frac{\partial^2 E}{\partial \varepsilon^2}\bigg|_{\varepsilon=0} \tag{8}$$

where $S = 2\pi R_n L$, with R_n being the tube radius and L the length of the tube cell. Our calculated values of Y_S for BeO nanotubes are reported in Table 1 and are consistent with those obtained at the LDA level.[15]

The elastic modulus is seen to be quite independent of tube size n. A comparison with the corresponding elastic constant C_{11} of the h-BeO monolayer is not straightforward. When a nanotube is stretched (compressed) in the axial direction, indeed, the radius reduces (increases) in order to minimize the total energy. In a corresponding deformation of the monolayer Poisson's effect has necessarily to be taken into account, that is, the deformation of a material orthogonally to the applied strain. As shown in Section 5, in the infinite radius limit, the Young modulus of the nanotubes tends to $(1 - \sigma^2)C_{11}$, where σ is Poisson's ratio. $(1 - \sigma^2)C_{11}$ = 0.137 TPa nm is then the value reported in the last row of Table 1.

The calculated values of the Young modulus are about 30% of those reported for Carbon nanotubes[65] and 40−50% of those reported for BN nanotubes[15,65] with the same radii: these are still rather high values, that make BeO nanotubes potentially interesting for the synthesis of highly resistant insulating composite materials.

BeO nanotubes also exhibit a longitudinal piezoelectric response, with the values reported in Table 1. The values are

dx.doi.org/10.1021/jp402340z | J. Phys. Chem. C 2013, 117, 12864−12872

Table 2. Vibration Wavenumbers $\bar{\nu} = \nu/c$ (cm^{-1}) and IR Intensities $\mathcal{I}$ (km/mol per BeO unit) of the IR Active Modes of the (n,0) Series of BeO Nanotubes[a]

	A1*		A2		A3*		B1*		B2		C1*		C2		C3*	
n	$\bar{\nu}$	$\mathcal{I}$	$\bar{\nu}$	$\mathcal{I}$	$\bar{\nu}$	$\mathcal{I}$	$\bar{\nu}$	$\mathcal{I}$	$\bar{\nu}$	$\mathcal{I}$	$\bar{\nu}$	$\mathcal{I}$	$\bar{\nu}$	$\mathcal{I}$	$\bar{\nu}$	$\mathcal{I}$
8	134.9	0.16	234.0	0.88	315.6	0.06	678.6	58.6	727.3	0.82	1002	0.09	1005	679	1161	291
10	108.3	0.12	188.8	0.54	259.0	0.03	687.8	57.4	725.2	0.49	1007	0.07	1009	681	1158	326
12	90.4	0.10	158.0	0.36	218.8	0.02	693.6	56.3	723.9	0.30	1010	0.05	1011	682	1150	356
14	77.5	0.08	135.8	0.27	189.1	0.01	697.6	55.4	723.1	0.20	1011	0.04	1012	682	1143	381
16	67.8	0.07	119.1	0.20	166.3	0.01	700.5	54.7	722.6	0.15	1012	0.03	1013	683	1135	403
20	54.3	0.05	95.4	0.13	133.9	0.00	704.5	53.6	721.8	0.09	1014	0.02	1014	683	1121	440
24	45.2	0.04	79.6	0.09	112.0	0.00	707.2	52.8	721.5	0.06	1014	0.01	1015	684	1109	468
32	33.9	0.02	59.8	0.05	84.3	0.00	710.7	51.7	721.2	0.03	1015	0.01	1015	684	1093	508
48	22.6	0.01	39.9	0.02	56.4	0.00	714.3	50.6	721.1	0.01	1015	0.01	1016	684	1072	556
64	16.9	0.01	29.9	0.01	42.3	0.00	716.0	50.0	721.1	0.01	1016	0.00	1016	684	1063	584

[a]Twofold degenerate modes are indicated with an asterisk.

about 25% higher with respect to BN nanotubes of comparable radii, which in turn are known to exhibit one of the largest piezoelectric response among low-dimensional systems.[66] The comparison of those values with that of the monolayer requires again to take into account Poisson's effect: the limit value is then $-(e_{11} - \sigma e_{12}) = -1.263$ au as shown in Section 5. The minus sign comes from the inversion of the x direction between slab and nanotube geometry.

Vibration Properties. As happens for single-walled nanotubes of any composition, the IR-active vibration modes of (n,0) BeO nanotubes can be subdivided into distinct groups, with their vibration frequencies ν tending to either an optical frequency of the monolayer or zero.[24] There are eight of these modes regardless of tube size: three modes are characterized by vanishing frequencies while increasing tube radius (to be referred to as A modes), two modes have vibration wavenumbers $\bar{\nu} = \nu/c$, with c the speed of light, that tend to 721 cm^{-1} (B modes), and three to 1016 cm^{-1} (C modes).

The vibration wavenumbers of the eight IR active modes of each tube are reported in Table 2 as well as their IR intensity, computed according to eq 2. In that table, all nondegenerate modes belong to the totally symmetric irreducible representation (irrep) of the group while all 2-fold degenerate modes, marked with an asterisk, belong to the same two-dimensional irrep. The most intense IR peaks correspond to modes C2, C3*, and B1*, following the notation introduced in Table 2. All B and C modes look very close to the corresponding monolayer optical modes and, with the exception of C3*, they are characterized by vibration frequencies almost independent of the tube size. The frequencies of the A modes decrease linearly with $1/n$ (see Figure 3) and tend to zero as n increases; these are collective modes without a direct correspondence in the vibrational spectrum of the h-BeO monolayer, as explained in what follows.

Collective Modes and Monolayer Elasticity. The A set contains three collective IR active modes: the first and third ones, A1* and A3*, are 2-fold degenerate (i.e., the two degenerate modes only differ by a permutation between atomic displacements along y and z). In A1*, Be and O atoms are both displaced toward $+x$ at the top of the ring and toward $-x$ at its bottom, x being the periodic direction of the tube. The overall dipole moment variation along x is null but minor displacements of the Be and O atoms produce a dipole moment in the yz plane. The A2 mode corresponds to ring breathing; while most of the vibration takes place in the yz plane, small opposite displacements of Be and O atoms along x make it slightly IR

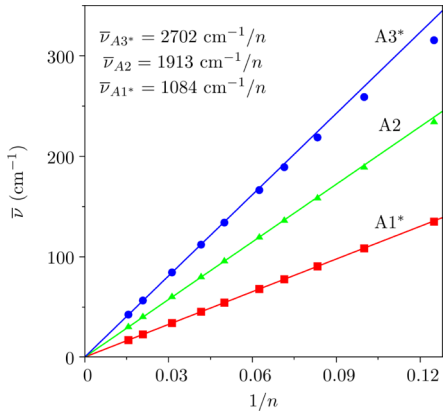

Figure 3. Vibration wavenumbers $\bar{\nu} = \nu/c$ of the A set of IR active modes as a function of $1/n$ in the (n,0) series of BeO nanotubes. The results of a linear fitting on the four largest tubes are shown as well.

active in the axial direction. The third mode, A3*, corresponds to the rigid clockwise rotation of half the ring in the yz plane and anticlockwise of the other half ring. It is slightly IR active in the yz plane. Due to their IR activity, these three modes contribute to the vibrational polarizability of the nanotube according to eq 4: however, only A1* and A2 contributions are nonvanishing in the limit of large tube radius.

It has recently been illustrated for BN nanotubes that, in the large radius limit, all these modes can be related to elastic deformations rather than to vibration modes of the monolayer.[24] The appearance of these vibration modes in the 1D nanotube structures can be interpreted in terms of the reduction of elastic degrees of freedom observed from a 2D to a 1D system. Due to hexagonal symmetry of the h-BeO monolayer, its elastic tensor $\mathbb{C}$ exhibits the following structure:

$$\mathbb{C} = \begin{vmatrix} C_{11} & C_{12} & 0 \\ C_{12} & C_{11} & 0 \\ 0 & 0 & \frac{1}{2}(C_{11} - C_{12}) \end{vmatrix} \quad (9)$$

The elements of this tensor are known as elastic constants. They have been computed with the fully automated procedure implemented in the CRYSTAL program[57] for the h-BeO monolayer where just two of them, C_{11} and C_{12}, are independent: $C_{11} = C_{22} = 2.223$ hartree and $C_{12} = 0.810$ hartree, so that $C_{66} = 1/2(C_{11} - C_{12}) = 0.707$ hartree.

dx.doi.org/10.1021/jp402340z | J. Phys. Chem. C 2013, 117, 12864−12872

By imposing equality between elastic and vibration strain energies, in the $n \rightarrow \infty$ limit, the coefficient of the linear behavior of these wavenumbers shown in Figure 3 can be expressed as a function of the elastic constants of the 2D monolayer: for instance, for the A1* and A2 modes we get

$$\nu_{A1*} = \sqrt{\frac{C_{66}}{(M_{Be} + M_O)}} \frac{1}{n|\mathbf{a}_2^{2D}|} \tag{10}$$

$$\nu_{A2} = \sqrt{\frac{C_{22}}{(M_{Be} + M_O)}} \frac{1}{n|\mathbf{a}_2^{2D}|} \tag{11}$$

where M_{Be} and M_O are the atomic masses of Be and O atoms and $\mathbf{a}_2^{2D}$ is the transverse lattice parameter of *h*-BeO. A similar expression holds for A3*: $\nu_{A3*} = \sqrt{2}\nu_{A2}$. The values resulting from this procedure are $\overline{\nu}_{A1*} = 1079.6/n$ cm^{-1}, $\overline{\nu}_{A2} = 1915.3/n$ cm^{-1} and $\overline{\nu}_{A3*} = 2708.6/n$ cm^{-1}, in agreement with those obtained by fitting the wavenumbers in Figure 3 for $n \geq 24$: $\overline{\nu}_{A1*} = 1084.3/n$ cm^{-1}, $\overline{\nu}_{A2} = 1913.2/n$ cm^{-1} and $\overline{\nu}_{A3*} = 2701.8/n$ cm^{-1}. Bearing in mind that the properties involved in the comparison (vibration frequencies of the nanotubes and elastic constants of the monolayer) are computed quite differently, agreement is remarkable.

Polarizability. In Table 1 we also report the values of the electronic and total static polarizability for the BeO nanotubes. The nuclear contribution to the polarizability, neglected in previous studies,[19] is here found to be as relevant as the electronic contribution in the low-frequency range, at variance with both carbon and BN nanotubes.[24]

The last row of Table 1 reports the corresponding monolayer (2D) limit values, to be defined in this section. The longitudinal component of electronic polarizability $\alpha_e^{\parallel}$ tends to the in-plane monolayer value. The static polarizability $\alpha_0^{\parallel}$ of the tubes contains the contribution due to mode A2, which is not present in the monolayer value. Analogously to the relationship between vibration frequencies and elasticity (discussed in Section 4), a connection can be established between the vibration contribution of collective modes to the polarizability and the monolayer piezoelectricity.[24] In this case:

$$\alpha_0^{\parallel}(n\rightarrow\infty) = \alpha_0^{\parallel}(2D) + \frac{e_{12}^2}{C_{22}} = (4.925 + 0.057)\ \text{Å}^3 \tag{12}$$

where e_{12} is a piezoelectric constant of *h*-BeO. As concerns the transverse component of the electronic nanotube polarizability $\alpha_e^{\perp}$, it can be shown by circular averaging[67] that in the large radius limit the following relation holds with the monolayer polarizability values:

$$\alpha_e^{\perp}(n\rightarrow\infty) = \frac{1}{2}[\alpha_e^{\perp}(2D) + \alpha_e^{\parallel}(2D)] \tag{13}$$

As in the case of $\alpha^{\parallel}$, in order to discuss the limit of the total static polarizability we need to take into account the contribution of the collective modes: that of A3* vanishes at $n \rightarrow \infty$ and is, in any case, negligible for all n values. The contribution of A1* is again connected with the piezoelectric properties of the monolayer, so that:

$$\begin{aligned}\alpha_0^{\perp}(n \rightarrow \infty) &= \frac{1}{2}[\alpha_0^{\perp}(2D) + \alpha_0^{\parallel}(2D)] + \frac{1}{2}\frac{e_{26}^2}{C_{66}} \\ &= \left(\frac{1}{2}(1.076 + 4.925) + 0.088\right)\text{Å}^3\end{aligned} \tag{14}$$

where $e_{26} = e_{12}$ is another piezoelectric constant of *h*-BeO.

A very satisfactory agreement is observed in the convergence as a function of n of all these properties. Figure 4 reports

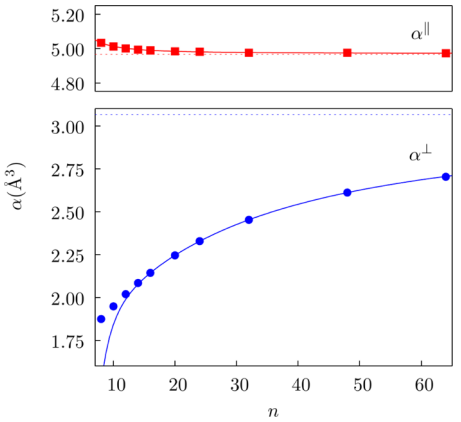

Figure 4. Longitudinal $\alpha^{\parallel}$ (upper panel) and transverse $\alpha^{\perp}$ (lower panel) total static polarizability of BeO nanotubes of the (n,0) family as a function of n. Also shown: the results of a fit with a third-order polynomial in ($1/n$) for the six largest tubes (solid lines), and monolayer limit values as defined in the text (dotted lines).

longitudinal (upper panel) and transverse (lower panel) total static polarizabilities of BeO nanotubes of the (n,0) family as a function of n. The corresponding monolayer limit values are reported as dotted lines. The longitudinal ($\alpha^{\parallel}$) components converge rapidly with n. The convergence of $\alpha^{\perp}$ is much slower, with a difference up to 40% for the smaller tubes.

4. CONCLUSIONS

This paper reports the results of an ab initio quantum chemical study of a variety of properties of single-walled zigzag beryllium oxide nanotubes, of the (n,0) family and, in particular, of their connection with the properties of the hexagonal monolayer (*h*-BeO). Nanotubes are investigated in the range from n = 8 (32 atoms in the unit cell and tube radius R = 3.4 Å) to 64 (256 atoms in the cell and R = 27.1 Å), that is, much larger radii than previously reported. Vibration frequencies, infrared (IR) intensities, piezoelectric constant, and nuclear contributions to the polarizability tensor are among the properties that are discussed here for the first time as concerns these materials. Rolling energy, elastic modulus, and electronic polarizability are also computed and discussed.

BeO nanotubes are confirmed to be wide band gap insulators with properties weakly dependent on the tube diameter and elastic moduli comparable with those of carbon nanotubes. Their piezoelectric response is also found to be large, making them suitable for nanoelectromechanical applications. The nuclear contribution to the static polarizability is comparable with the electronic one.

Recent improvements in the CRYSTAL program permit full use of symmetry (the point group contains as many symmetry operators as atoms in the unit cell) and to drastically reduce

dx.doi.org/10.1021/jp402340z | J. Phys. Chem. C 2013, 117, 12864−12872

computational cost. Thus, we can perform accurate simulations of much larger tubes than before and improve the description of the convergence of a variety of tube properties to the flat monolayer. From a careful analysis of such convergences, connections are established between physical properties of nanotubes and flat monolayer: the relationship between a particular set of IR-active vibration modes of the nanotubes, with vanishing vibration frequency as a function of n, and the elastic and piezoelectric constants of h-BeO is illustrated and discussed.

IR-active vibration modes are separated into three distinct sets. The first set, in the 0−300 cm^{-1} frequency range, is characterized by vanishing vibration frequencies at infinite R while their IR intensities do not vanish; the nature of these normal modes is illustrated by establishing a connection between them and the elastic and piezoelectric constants of h-BeO. The second (680−730 cm^{-1}) and third (1000−1200 cm^{-1}) sets tend regularly to the optical modes of the monolayer.

5. CONNECTION BETWEEN NANOTUBES AND MONOLAYER ELASTIC CONSTANTS

The definition of elastic constants given in eq 5 takes into account relaxation of the nuclei upon strain, thus allowing to go beyond the so-called "clamped ion" approximation,[68,69] but not that of the lattice parameters orthogonally to applied strain (Poisson effect). It follows that, when strain ε_1 is applied to a monolayer, no relaxation of the cell can occur in the transverse direction; the case is different for a nanotube where the application of ε_1 still allows to the system, to relax along the transverse direction (i.e., to change the tube radius). When comparing the $n \rightarrow \infty$ limit of the nanotube with the monolayer, we must consider that the 1D limit includes Poisson's effect whereas the monolayer does not. The monolayer elastic value has to be modified according to Poisson's ratio:[70,71]

$$\sigma = \frac{d\varepsilon_2}{d\varepsilon_1} = -\frac{C_{12}}{C_{22}} \tag{15}$$

We can use the total derivative theorem to obtain the derivative of the energy with respect to the strain applied to the monolayer, including Poisson's effect:

$$\frac{dE(\varepsilon_1, \varepsilon_2(\varepsilon_1))}{d\varepsilon_1} = \frac{\partial E}{\partial \varepsilon_1} + \frac{\partial E}{\partial \varepsilon_2}\frac{d\varepsilon_2}{d\varepsilon_1} = \frac{\partial E}{\partial \varepsilon_1} + \frac{\partial E}{\partial \varepsilon_2}\sigma \tag{16}$$

Since we are here interested in calculating how Poisson's effect affects the C_{11} elastic constant of h-BeO, we work out the following second derivative of the energy:

$$\begin{aligned}\frac{d^2E}{d\varepsilon_1^2} &= \frac{\partial}{\partial \varepsilon_1}\left(\frac{\partial E}{\partial \varepsilon_1} + \sigma\frac{\partial E}{\partial \varepsilon_2}\right) + \sigma\frac{\partial}{\partial \varepsilon_2}\left(\frac{\partial E}{\partial \varepsilon_1} + \sigma\frac{\partial E}{\partial \varepsilon_2}\right)\\ &= \frac{\partial^2 E}{\partial \varepsilon_1^2} + 2\sigma\frac{\partial^2 E}{\partial \varepsilon_1 \partial \varepsilon_2} + \sigma^2\frac{\partial^2 E}{\partial \varepsilon_2^2}\\ &= C_{11} + 2\sigma C_{12} + \sigma^2 C_{22}\\ &= C_{11} - 2\frac{C_{12}^2}{C_{22}} + \left(\frac{C_{12}}{C_{22}}\right)^2 C_{22}\\ &= C_{11} - \frac{C_{12}^2}{C_{22}}\end{aligned} \tag{17}$$

The BeO monolayer is isotropic in the layer plane, that is, $C_{11} \equiv C_{22}$. It then follows that:

$$\frac{d^2E}{d\varepsilon_1^2} = C_{11}(1 - \sigma^2) \tag{18}$$

The Poisson-corrected monolayer value turns out to be C_{11}, damped by a factor $(1 - \sigma^2)$. For h-BeO, with $C_{11} = 2.223$ hartree and $C_{12} = 0.810$ hartree, we obtain $|\sigma| = 0.364$ and $(1 - \sigma^2) = 0.8672$. The damping effect is significant in this case due to the relatively high ionicity of the Be−O bond. It is worth mentioning that $|\sigma_C| < |\sigma_{BN}| < |\sigma_{BeO}|$, so that for carbon and BN monolayers the $(1 - \sigma^2)$ correction is almost negligible, amounting to factors of 0.970 and 0.955, respectively.

Similarly, when considering the piezoelectric effect in a nanotube we must take into account the variation of the polarization vector due to the relaxation of the tube radius. Analogously to eq 16, the corresponding monolayer property is then:

$$\frac{dP_x(\varepsilon_1, \varepsilon_2(\varepsilon_1))}{d\varepsilon_1} = \frac{\partial P_x}{\partial \varepsilon_1} + \frac{\partial P_x}{\partial \varepsilon_2}\frac{d\varepsilon_2}{d\varepsilon_1} = \frac{\partial P_x}{\partial \varepsilon_1} + \frac{\partial P_x}{\partial \varepsilon_2}\sigma \tag{19}$$

where x is the monolayer direction corresponding to the longitudinal direction of the nanotube. Then:

$$\frac{dP_x}{d\varepsilon_1} = e_{11} - \frac{C_{12}}{C_{11}}e_{12} \tag{20}$$

according to the definition of piezoelectric constants in eq 6.

AUTHOR INFORMATION

Corresponding Author

*E-mail: roberto.dovesi@unito.it.

Notes

The authors declare no competing financial interest.

ACKNOWLEDGMENTS

The authors acknowledge the CINECA Award N. HP10BLSOR4-2012 for the availability of high-performance computing resources and support.

REFERENCES

(1) Ijima, S. Helical Microtubules of Graphitic Carbon. *Nature* **1991**, *354*, 56−58.
(2) Kahaly, M. U.; Waghmare, U. V. Vibrational Properties of Single-Wall Carbon Nanotubes: A First-Principles Study. *J. Nanosci. Nanotechnol.* **2007**, *7*, 1787−1792.
(3) Harris, P. J. F. *Carbon Nanotubes and Related Structures: New Materials for the Twenty-first Century*; Cambridge University Press: Cambridge, UK, 1999.
(4) Ivanovskii, A. L. Non-carbon Nanotubes: Synthesis and Simulation. *Russ. Chem. Rev.* **2002**, *71*, 203.
(5) Tenne, R.; Rao, C. N. R. Inorganic Nanotubes. *Philos. Trans. R. Soc., A* **2004**, *362*, 2099.
(6) Barth, S.; Hernandez-Ramirez, F.; Holmes, J. D.; Romano-Rodriguez, A. Synthesis and Applications of One-dimensional Semiconductors. *Prog. Mater. Sci.* **2010**, *55*, 563−627.
(7) Lu, J. G.; Chang, P.; Fan, Z. Quasi-one-dimensional Metal Oxide Materials: Synthesis, Properties and Applications. *Mater. Sci. Eng., R* **2006**, *52*, 49−91.
(8) Comini, E.; Baratto, C.; Faglia, G.; Ferroni, M.; Vomiero, A.; Sberveglieri, G. Quasi-one Dimensional Metal Oxide Semiconductors: Preparation, Characterization and Application as Chemical Sensors. *Prog. Mater. Sci.* **2009**, *54*, 1−67.

(9) Lichanot, A.; Chaillet, M.; Larrieu, C.; Dovesi, R.; Pisani, C. Ab initio Hartree-Fock Study of Solid Beryllium Oxide: Structure and Electronic Properties. *Chem. Phys.* **1992**, *164*, 383−394.
(10) Ivanovskii, A.; Shein, I.; Makurin, Y.; Kiiko, V.; Gorbunova, M. Electronic Structure and Properties of Beryllium Oxide. *Inorg. Mater.* **2009**, *45*, 223−234.
(11) Kingery, W. D.; Franch, J.; Coble, R. L.; Vasilos, T. Thermal Conductivity: X, Data for Several Pure Oxide Materials Corrected to Zero Porosity. *J. Am. Ceram. Soc.* **1954**, *37*, 107−110.
(12) Campbell, I. E. *High-temperature technology*; Wiley: New York, NY, 1956.
(13) Continenza, A.; Wentzcovitch, R. M.; Freeman, A. J. Theoretical Investigation of Graphitic BeO. *Phys. Rev. B* **1990**, *41*, 3540−3544.
(14) Sorokin, P. B.; Fedorov, A. S.; Chernozatonskii, L. A. Structure and Properties of BeO Nanotubes. *Phys. Solid State* **2006**, *48*, 398−401.
(15) Baumeier, B.; Kruger, P.; Pollmann, J. Structural, Elastic, and Electronic Properties of SiC, BN, and BeO Nanotubes. *Phys. Rev. B* **2007**, *76*, 085407.
(16) Gorbunova, M. A.; Shein, I. R.; Makurin, Y. N.; Ivanovskaya, V. V.; Kijko, V. S.; Ivanovskii, A. L. Electronic Structure and Magnetism in BeO Nanotubes Induced by Boron, Carbon and Nitrogen Doping, and Beryllium and Oxygen Vacancies Inside Tube Walls. *Physica E* **2008**, *41*, 164−168.
(17) Roozbahani, G. M.; Seif, A. A Computational NMR Study of Nitrogen Substitutional Impurity in the Armchair BeO Nanotube. *Superlattices Microstruct.* **2012**, *51*, 363−371.
(18) Ma, L.-C.; Zhao, H.-S.; Yan, W.-J. Structural, Electronic and Magnetic Properties of Linear Monoatomic Chains Adsorption on Beryllium Oxide Nanotube: First-principle Study. *J. Magn. Magn. Mater.* **2013**, *330*, 174−180.
(19) Fathalian, A.; Moradian, R.; Shahrokhi, M. Optical Properties of BeO Nanotubes: Ab initio Study. *Solid State Commun.* **2013**, *156*, 1−7.
(20) Becke, A. D. Density Functional Theochemistry. III The Role of Exact Exchange. *J. Chem. Phys.* **1993**, *98*, 5648−5652.
(21) Lee, C.; Yang, W.; Parr, R. G. Development of the Colle-Salvetti Correlation-Energy Formula into a Functional of the Electron Density. *Phys. Rev. B* **1988**, *37*, 785−789.
(22) Noël, Y.; D'Arco, P.; Demichelis, R.; Zicovich-Wilson, C.; Dovesi, R. On the Use of Symmetry in the Ab initio Quantum Mechanical Simulation of Nanotubes and Related Materials. *J. Comput. Chem.* **2010**, *31*, 855−862.
(23) Demichelis, R.; Noël, Y.; D'Arco, P.; Rérat, M.; Zicovich-Wilson, C.; Dovesi, R. Properties of Carbon Nanotubes: An Ab initio Study Using Large Gaussian Basis Sets and Various DFT Functionals. *J. Phys. Chem. C* **2011**, *115*, 8876−8885.
(24) Erba, A.; Ferrabone, M.; Baima, J.; Orlando, R.; Rérat, M.; Dovesi, R. The Vibration Properties of the (*n*,0) Boron Nitride Nanotubes from *Ab initio* Quantum Chemical Simulations. *J. Chem. Phys.* **2013**, *138*, 054906.
(25) Orlando, R.; Bast, R.; Ruud, K.; Ekström, U.; Ferrabone, M.; Kirtman, B.; Dovesi, R. The First and Second Static Electronic Hyperpolarizabilities of Zigzag Boron Nitride Nanotubes. An Ab initio Approach through the Coupled Perturbed Kohn-Sham Scheme. *J. Phys. Chem. A* **2011**, *115*, 12631−12637.
(26) Ferrabone, M.; Kirtman, B.; Rérat, M.; Orlando, R.; Dovesi, R. Polarizability and Hyperpolarizability of BN Zigzag Nanotubes Calculated by the Coupled Perturbed Kohn-Sham Scheme. *Phys. Rev. B* **2011**, *83*, 235421.
(27) Ferrabone, M.; Kirtman, B.; Lacivita, V.; Rérat, M.; Orlando, R.; Dovesi, R. Vibrational Contribution to Static and Dynamic (Hyper)-Polarizabilities of Zigzag BN Nanotubes Calculated by the Finite Field Nuclear Relaxation Method. *Int. J. Quantum Chem.* **2012**, *112*, 2160−2170.
(28) Lacivita, V.; Erba, A.; Noël, Y.; Orlando, R.; D'Arco, P.; Dovesi, R. Zinc Oxide Nanotubes: An *Ab initio* Investigation of their Structural, Vibrational, Elastic and Dielectric Properties. *J. Chem. Phys.* **2013**, *138*, 214706.
(29) Demichelis, R.; Noël, Y.; D'Arco, Ph.; Maschio, L.; Orlando, R.; Dovesi, R. Structure and Energetics of Imogolite: A Quantum Mechanical Ab initio Study with B3LYP Hybrid Functional. *J. Mater. Chem.* **2010**, *20*, 10417−10425.
(30) D'Arco, P.; Noël, Y.; Demichelis, R.; Dovesi, R. Single-layered Chrysotile Nanotubes: A Quantum Mechanical Ab initio Simulation. *J. Chem. Phys.* **2009**, *131*, 204701.
(31) Dovesi, R.; Saunders, V. R.; Roetti, C.; Orlando, R.; Zicovich-Wilson, C. M.; Pascale, F.; Doll, K.; Harrison, N. M.; Civalleri, B.; Bush, I. J.; D'Arco, P.; Llunell, M. CRYSTAL09 User's Manual, 2009.
(32) Dovesi, R.; Orlando, R.; Civalleri, B.; Roetti, C.; Saunders, V. R.; Zicovich-Wilson, C. M. CRYSTAL: A Computational Tool for the Ab initio Study of the Electronic Properties of Crystals. *Z. Kristallogr.* **2005**, *220*, 571−573.
(33) The basis set can be found at http://www.crystal.unito.it/Basis_Sets/beryllium.html, http://www.crystal.unito.it/Basis_Sets/oxygen.html.
(34) Doll, K. Implementation of Analytical Hartree-Fock Gradients for Periodic Systems. *Comput. Phys. Commun.* **2001**, *137*, 74−88.
(35) Doll, K.; Harrison, N. M.; Saunders, V. R. Analytical Hartree-Fock Gradients for Periodic Systems. *Int. J. Quantum Chem.* **2001**, *82*, 1−13.
(36) Civalleri, B.; D'Arco, P.; Orlando, R.; Saunders, V. R.; Dovesi, R. Hartree-Fock Geometry Optimization of Periodic Systems with the CRYSTAL Code. *Chem. Phys. Lett.* **2001**, *348*, 131−138.
(37) Broyden, C. G. The Convergence of a Class of Double-rank Minimization Algorithms 1. General Considerations. *J. Inst. Math. Its Appl.* **1970**, *6*, 76−90.
(38) Fletcher, R. A New Approach to Variable Metric Algorithms. *Comput. J.* **1970**, *13*, 317−322.
(39) Goldfarb, D. A Family of Variable-Metric Methods Derived by Variational Means. *Math. Comput.* **1970**, *24*, 23−26.
(40) Shanno, D. F. Conditioning of Quasi-Newton Methods for Function Minimization. *Math. Comput.* **1970**, *24*, 647−656.
(41) Pascale, F.; Zicovich-Wilson, C. M.; Gejo, F. L.; Civalleri, B.; Orlando, R.; Dovesi, R. The Calculation of the Vibrational Frequencies of Crystalline Compounds and its Implementation in the CRYSTAL Code. *J. Comput. Chem.* **2004**, *25*, 888−897.
(42) Zicovich-Wilson, C. M.; Pascale, F.; Roetti, C.; Saunders, V. R.; Orlando, R.; Dovesi, R. The Calculation of the Vibration Frequencies of α-Quartz: The Effect of Hamiltonian and Basis Set. *J. Comput. Chem.* **2004**, *25*, 1873−1881.
(43) Pascale, F.; Zicovich-Wilson, C. M.; Orlando, R.; Roetti, C.; Ugliengo, P.; Dovesi, R. Vibration Frequencies of $Mg_3Al_2Si_3O_{12}$ Pyrope. An Ab Initio Study with the CRYSTAL Code. *J. Phys. Chem. B* **2005**, *109*, 6146−6152.
(44) Carteret, C.; De La Pierre, M.; Dossot, M.; Pascale, F.; Erba, A.; Dovesi, R. The Vibrational Spectrum of $CaCO_3$ Aragonite: A Combined Experimental and Quantum-mechanical Investigation. *J. Chem. Phys.* **2013**, *138*, 014201.
(45) Erba, A.; Casassa, S.; Dovesi, R.; Maschio, L.; Pisani, C. Periodic Density Functional Theory and Local-MP2 Study of the Librational Modes of Ice XI. *J. Chem. Phys.* **2009**, *130*, 074505.
(46) Barrow, G. M. *Introduction to molecular spectroscopy*; McGraw-Hill: New York, NY, 1962; Chapter 4, p 70.
(47) Hess, B. A.; Schaad, L. J.; Carsky, P.; Zahradnik, R. Ab Initio Calculations of Vibrational Spectra and Their Use in the Identification of Unusual Molecules. *Chem. Rev.* **1986**, *86*, 709−730.
(48) Baranek, P.; Zicovich-Wilson, C. M.; Roetti, C.; Orlando, R.; Dovesi, R. Well Localized Crystalline Orbitals Obtained from Bloch Functions: The Case of $KNbO_3$. *Phys. Rev. B* **2001**, *64*, 125102.
(49) Noël, Y.; Zicovich-Wilson, C. M.; Civalleri, B.; D'Arco, P.; Dovesi, R. Polarization Properties of ZnO and BeO: An *Ab initio* Study through the Berry Phase and Wannier Functions Approaches. *Phys. Rev. B* **2002**, *65*, 014111.
(50) Zicovich-Wilson, C. M.; Torres, F. J.; Pascale, F.; Valenzano, L.; Orlando, R.; Dovesi, R. *Ab initio* Simulation of the IR Spectra of Pyrope, Grossular and Andradite. *J. Comput. Chem.* **2008**, *29*, 2268−2278.

(51) Hurst, G. J. B.; Dupuis, M.; Clementi, E. Ab initio Analytic Polarizability, First and Second Hyperpolarizabilities of Large Conjugated Organic Molecules: Applications to Polyenes C_4H_6 to $C_{22}H_{24}$. *J. Chem. Phys.* **1988**, *89*, 385−395.
(52) Kirtman, B.; Gu, F. L.; Bishop, D. M. Extension of the Genkin and Mednis Treatment for Dynamic Polarizabilities and Hyperpolarizabilities of Infinite Periodic Systems. I. Coupled Perturbed Hartree-Fock Theory. *J. Chem. Phys.* **2000**, *113*, 1294−1309.
(53) Ferrero, M.; Rérat, M.; Orlando, R.; Dovesi, R. The Calculation of Static Polarizabilities of Periodic Compounds. The Implementation in the CRYSTAL Code for 1D, 2D and 3D Systems. *J. Comput. Chem.* **2008**, *29*, 1450−1459.
(54) Ferrero, M.; Rérat, M.; Orlando, R.; Dovesi, R. Coupled Perturbed Hartree-Fock for Periodic Systems: The Role of Symmetry and Related Computational Aspects. *J. Chem. Phys.* **2008**, *128*, 014110.
(55) Ferrero, M.; Rérat, M.; Orlando, R.; Dovesi, R. *Coupled Perturbed Hartree-Fock Calculation of the Static Polarizability for Periodic Systems: Implementation in the CRYSTAL Code*; AIP Conference Proceedings; Simos, T. E.; Maroulis, G. American Institute of Physics, 2007; Computation in Modern Science and Engineering, Vol. *2B*; pp 1199−1203.
(56) Kirtman, B.; Lacivita, V.; Dovesi, R.; Reis, H. Electric Field Polarization in Conventional Density Functional Theory: From Quasilinear to Two-dimensional and Three-dimensional Extended Systems. *J. Chem. Phys.* **2011**, *135*, 154101.
(57) Perger, W. F.; Criswell, J.; Civalleri, B.; Dovesi, R. Ab initio Calculation of Elastic Constants of Crystalline Systems with the CRYSTAL Code. *Comput. Phys. Commun.* **2009**, *180*, 1753−1759.
(58) Nye, J. F. *Physical properties of crystals*; Oxford University Press: Oxford, UK, 1957.
(59) Noël, Y.; Llunell, M.; Orlando, R.; D'Arco, P.; Dovesi, R. Performance of Various Hamiltonians In the Study of the Piezoelectric Properties of Crystalline Compounds: The Case of BeO and ZnO. *Phys. Rev. B* **2002**, *66*, 214107.
(60) Catti, M.; Noël, Y.; Dovesi, R. Full Piezoelectric Tensors of Wurtzite and Zinc Blende ZnO and ZnS by First-principles Calculations. *J. Phys. Chem. Solids* **2003**, *64*, 2183.
(61) Canepa, P.; Hanson, R.; Ugliengo, P.; Alfredsson, M. J-ICE: A New Jmol Interface for Handling and Visualizing Crystallographic and Electronic Properties. *J. Appl. Crystallogr.* **2011**, *44*, 225−229.
(62) Weber, M. J. *Handbook of Laser Science and Technology*; CRC Press: New York, NY, 1986; Vol. *3*.
(63) Tibbetts, G. G. Why are Carbon Filaments Tubular? *J. Cryst. Growth* **1984**, *66*, 632−638.
(64) Robertson, D. H.; Brenner, D. W.; Mintmire, J. W. Energetics of Nanoscale Graphitic Tubules. *Phys. Rev. B* **1992**, *45*, 12592−12595.
(65) Hernández, E.; Goze, C.; Bernier, P.; Rubio, A. Elastic Properties of C and $B_xC_yN_z$ Composite Nanotubes. *Phys. Rev. Lett.* **1998**, *80*, 4502−4505.
(66) Nakhmanson, S. M.; Calzolari, A.; Meunier, V.; Bernholc, J.; Nardelli, M. B. Spontaneous Polarization and Piezoelectricity in Boron Nitride Nanotubes. *Phys. Rev. B* **2003**, *67*, 235406.
(67) Guo, G. Y.; Ishibashi, S.; Tamura, T.; Terakura, K. Static Dielectric Response and Born Effective Charge of BN Nanotubes from *Ab initio* Finite Electric Field Calculations. *Phys. Rev. B* **2007**, *75*, 245403.
(68) Saghi-Szabo, G.; Cohen, R. E.; Krakauer, H. First-Principles Study of Piezoelectricity in $PbTiO_3$. *Phys. Rev. Lett.* **1998**, *80*, 4321−4324.
(69) Dal Corso, A.; Posternak, M.; Resta, R.; Baldereschi, A. Ab initio Study of Piezoelectricity and Spontaneous Polarization in ZnO. *Phys. Rev. B* **1994**, *50*, 10715.
(70) Landau, L. D.; Lifshitz, E. M. *Theory of Elasticity, Course of Theoretical Physics*; Pergamon Press: Oxford, UK, 1986.
(71) Sánchez-Portal, D.; Hernández, E. Vibrational Properties of Single-wall Nanotubes and Monolayers of Hexagonal BN. *Phys. Rev. B* **2002**, *66*, 235415.